Mechanism study on electromagnetic acoustic transducer for ultrasonic generation in ferromagnetic material

Lei Huaming Que Peiwen Zhang Zhigang Huang Jing

(Institute of Automatic Detection, Shanghai Jiaotong University, Shanghai 200030, China)

Abstract: Based on the proper assumptions and approximations, the coupling mechanism of the electromagnetic acoustic transducer (EMAT) for ultrasonic generation within ferromagnetic material has been studied by analyzing the eddy current distribution, Lorentz force, magnetostriction force and magnetization force. Some useful numerical calculations are presented to explain the EMAT behavior with general geometric arrangements. It is indicated that for the ferromagnetic material the magnetostriction effect dominates the EMAT phenomenon for ultrasonic wave generation in low magnetic field intensity, while the material has not reached its magnetizing saturation. But, with the bias magnetic field increasing and saturation, the magnetostrictive terms will make no contributions to the ultrasonic generation and the Lorentz force becomes the only exciting mechanism. It is important to determine both the Lorentz and magnetostriction forces and select the appropriate working manner for achieving an optimized design.

Key words: electromagnetic acoustic transducer (EMAT); ferromagnetic material; ultrasonic generation; eddy current; Lorentz force; magnetostriction force

Electromagnetic acoustic transducer (EMAT) has been proved to be powerful for industrial purposes because of its robustness, its omission of surface preparations and its capacity for simple measurement in a short time[1-7]. Many researches have emphasized the modeling and application of EMAT. Previous works[8,9] have concluded that three mechanisms are responsible for the coupling. They are the Lorentz force mechanism due to the interaction between induced eddy current and the bias magnetic field, the magnetization effect due to the bias magnetization, and the magnetostriction mechanism due to the piezomagnetic effect.

For nonmagnetic metal, ultrasonic generation is well understood as the Lorentz force mechanism only and its amplitude is proportional to the static field strength. However, for a ferromagnetic metal, the signal amplitude is no longer proportional to the static field strength since the magnetostriction becomes important, especially in the low magnetic field region, and even phase inversion may occur[10]. As the mechanism of EMAT for ferromagnetic metal NDT is complex and not very clear, it creates an obstacle to the proper design and effective use of EMAT. It is important to study the mechanism of the EMAT to get the maximum transduction.

Fig. 1 shows the different kinds of forces and their directions which are coupled in ultrasonic generation. The elastic wave field in the ferromagnetic metal is based on an electromagnetic body force $\boldsymbol{f}$ of per unit volume, which can be expressed as the summation of Lorentz force $\boldsymbol{f}_{\mathrm{L}}$, magnetization force $\boldsymbol{f}_{\mathrm{M}}$, and magnetostriction force $\boldsymbol{f}_{\mathrm{MS}}$[8,9],

$$\boldsymbol{f} = \boldsymbol{f}_{\mathrm{L}} + \boldsymbol{f}_{\mathrm{MS}} + \boldsymbol{f}_{\mathrm{M}} \tag{1}$$

$$\boldsymbol{f}_{\mathrm{L}} = \boldsymbol{J}_{\mathrm{e}} \times \boldsymbol{B}_0 \tag{2}$$

$$\boldsymbol{f}_{\mathrm{M}} = (\nabla \boldsymbol{H}) \cdot \boldsymbol{M}_0 \tag{3}$$

$$\boldsymbol{f}_{\mathrm{MS}} = \nabla \cdot (\boldsymbol{e} \cdot \boldsymbol{H}) \tag{4}$$

where $\boldsymbol{J}_{\mathrm{e}}$ is the eddy current density caused by the source current density $\boldsymbol{J}$ in the EMAT coil, $\boldsymbol{e}$ is the tensor of magnetostriction, $\boldsymbol{B}_0$ and $\boldsymbol{M}_0$ are the static magnetic flux density and static magnetization vector, and $\boldsymbol{H}$ is the magnetic field.

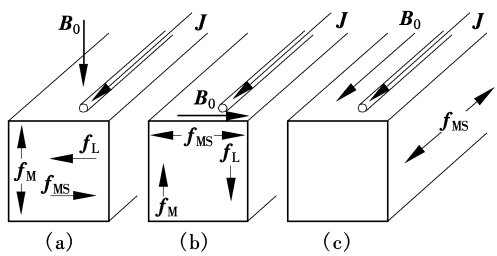

Fig.1 Ultrasonic generation mechanisms of EMAT

The acoustic field equation can be stated in terms of a particle displacement vector $\boldsymbol{u}$ and the body force $\boldsymbol{f}$ as follows:

$$\frac{\partial^2 \boldsymbol{u}}{\partial t^2} = c_{\mathrm{L}}^2 \nabla \nabla \cdot \boldsymbol{u} - c_{\mathrm{S}}^2 \nabla \times \nabla \times \boldsymbol{u} + \rho^{-1} \boldsymbol{f} \tag{5}$$

$$c_{\mathrm{L}}^2 = \frac{\lambda + 2\mu}{\rho}, \quad c_{\mathrm{S}}^2 = \frac{\mu}{\rho} \tag{6}$$

Received 2004-02-24.

Foundation item: The National High Technology Research and Development Program of China (863 Program) (No. 2001AA602021).

Biographies: Lei Huaming (1976—), male, graduate; Que Peiwen (corresponding author), female, professor, pwque@sjtu.edu.cn.

where ρ is the mass volume density, λ and μ are the Lamé constants, c_L and c_S are the longitudinal and shear sound velocities, respectively.

1 Assumptions and Approximations

A meandering planar coil EMAT with parallel wires and static magnetic field, which is normal to the surface, is shown in Fig.2.

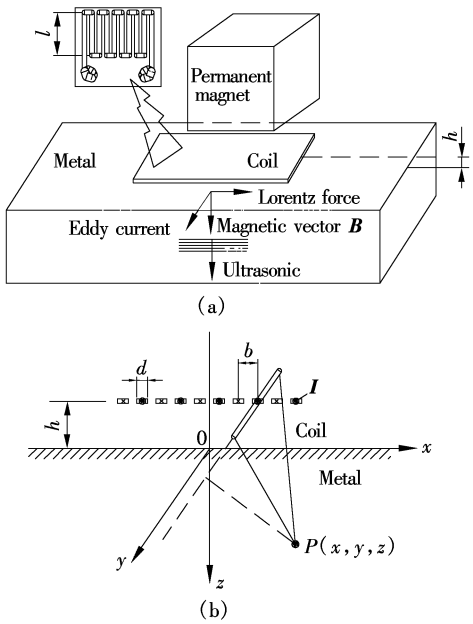

Fig.2 Geometry used for the theoretical calculation. (a) Solid view; (b) Cross section and coordination system

The inspected metal is assumed to be a semi-infinite ferromagnetic conducting medium (e.g. low carbon steel). The coil is located near the surface with a lift-off h, and driven by radio frequency (RF) current $I = I_0 \exp(j\omega t)$, where ω is the angular frequency. For simplification, the edge effect of the meandering coil is assumed to be omitted, the wire width d is much smaller than the wire space b, and the metal is an isotropic metal. The bias field is homogeneous being normal to the surface and the magnetostriction causes only iso-volume change. Another assumption is that the system is considered as quasi-stationary case because the physical size of the system is much smaller than the electromagnetic wavelength. Based on the approximations, the following parts discuss the coupling mechanisms of the EMAT.

2 Eddy Current Distribution, Lorentz Force and Magnetization Force

In order to determine the Lorentz force in Eq.(2), it is essential to firstly establish the eddy current density distribution. When only considering the ultrasonic exciting process, the eddy current density distribution can be expressed as

$$\boldsymbol{J}_e = \sigma \boldsymbol{E} \tag{7}$$

For solving the electromagnetic field, the magnetic vector potential $\boldsymbol{A}$ is introduced as

$$\boldsymbol{B} = \nabla \times \boldsymbol{A} \tag{8}$$

According to Maxwell theories and the vector principle, the electric field can be expressed in terms of the time derivative of the magnetic vector potential,

$$\boldsymbol{E} = -\frac{\partial \boldsymbol{A}}{\partial t} \tag{9}$$

A parabolic partial differential equation about $\boldsymbol{A}$ is obtained as

$$\frac{\nabla^2 \boldsymbol{A}}{\mu} - \sigma \frac{\partial \boldsymbol{A}}{\partial t} = -\boldsymbol{J} \tag{10}$$

The induced eddy current density distribution $\boldsymbol{J}_e$ in the metal is

$$\boldsymbol{J}_e = -\sigma \frac{\partial \boldsymbol{A}}{\partial t} \tag{11}$$

The boundary conditions in terms of the normal and tangential components of the magnetic induction and magnetic field can be expressed as vector potentials as follows:

$$\hat{\boldsymbol{n}} \cdot (\boldsymbol{B}_{\text{metal}} - \boldsymbol{B}_{\text{air}}) = 0 \tag{12}$$

$$\hat{\boldsymbol{n}} \times (\boldsymbol{H}_{\text{metal}} - \boldsymbol{H}_{\text{air}}) = \boldsymbol{J}_s \tag{13}$$

where $\boldsymbol{J}_s$ is the surface current density on the metal surface.

Based on the aforementioned assumptions, the electromagnetic fields will be approximated to be governed by the classical skin effect. They consist of a static magnetic field ($H_0\hat{z}$) and dynamic fields. The electromagnetic field generated with each straight wire which is in $\hat{y}$ direction can be calculated using the superposition principles. The components of dynamic field intensity of point $P(x, y, z)$ in the metal can be approximately expressed as

$$H_x = \sum_{m=-k}^{k-1} (-1)^m \left[\frac{2\mu_1}{\mu_1 + \mu_2} \frac{I_0 \exp(j\omega t) \exp(-(1+j)z/\delta)}{4\pi\gamma} \cdot \left(\frac{y + l/2}{\sqrt{\gamma^2 + (y + l/2)^2}} - \frac{y - l/2}{\sqrt{\gamma^2 + (y - l/2)^2}} \right) \frac{x - r}{\gamma} \right] \quad z \geqslant 0 \tag{14}$$

$$H_z = \sum_{m=-k}^{k-1} (-1)^m \left[\frac{2\mu_1}{\mu_1 + \mu_2} \frac{I_0 \exp(j\omega t) \exp(-(1+j)z/\delta)}{4\pi\gamma} \cdot \frac{y + l/2}{\sqrt{\gamma^2 + (y + l/2)^2}} - \frac{y - l/2}{\sqrt{\gamma^2 + (y - l/2)^2}} \right) \frac{z + h}{\gamma} \right] \quad z \geqslant 0 \tag{15}$$

$$H_y = 0$$

where $\gamma = \sqrt{(x - r)^2 + (z + h)^2}$, $r = b(2m + 1)/2$, $(m = -k, \cdots, k - 1)$, $2k$ is the total turns of the coil, μ_1 and μ_2 are the relative permeabilities of the air and metal, respectively, and δ is the electromagnetic skin depth given by

$$\delta = \sqrt{2/(\mu_0 \mu_2 \omega \sigma)} \tag{16}$$

where σ is the electrical conductivity.

The dynamic magnetization and eddy current density can be written as

$$M_x = \mu_0 \mu_x H_x \tag{17}$$

$$M_z = \mu_0 \mu_z H_z \tag{18}$$

$$\boldsymbol{J}_e = \nabla \times \boldsymbol{H} = \frac{\partial H_z}{\partial y}\hat{\boldsymbol{x}} + \left(\frac{\partial H_x}{\partial z} - \frac{\partial H_z}{\partial x}\right)\hat{\boldsymbol{y}} - \frac{\partial H_x}{\partial y}\hat{\boldsymbol{z}} \tag{19}$$

and from Eqs. (2) and (3), the Lorentz force and magnetization force can be written as

$$\boldsymbol{f}_L = -\mu H_0 \left(\frac{\partial H_z}{\partial y}\right)\hat{\boldsymbol{y}} + \mu H_0 \left(\frac{\partial H_x}{\partial z} - \frac{\partial H_z}{\partial x}\right)\hat{\boldsymbol{x}} \tag{20}$$

$$\boldsymbol{f}_M = M_0 \left(\frac{\partial H_z}{\partial x}\hat{\boldsymbol{x}} + \frac{\partial H_z}{\partial y}\hat{\boldsymbol{y}} + \frac{\partial H_z}{\partial z}\hat{\boldsymbol{z}}\right) \tag{21}$$

These forces transfer to the lattice and generate elastic waves through collision and interaction.

3 Magnetostriction Force

The magnetic anisotropy is induced under the bias field by reason of the rotation of magnetization and the movement of magnetic domain walls. As an inspected metal, such as low carbon steel, its magnetization and magnetostriction properties are demonstrated by Eqs. (22) and (23) and Fig. 3[8].

Magnetization M to the field H:

$$M = 2.2(0.27 - 0.73\tanh(0.38 - 8.6H)) \tag{22}$$

Magnetostriction ε_{MS} to the field H:

$$\varepsilon_{MS} = 8H^{0.395} \cdot 1.79^{(-10H+1)} - 0.75 \tag{23}$$

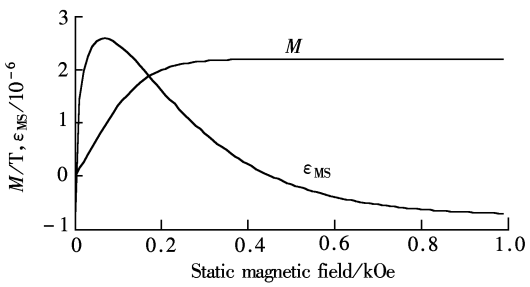

Fig.3 Magnetization and magnetostriction curves for a low carbon steel

A change in the magnetization of a ferromagnet in a magnetic field causes a deformation in it. Magnetostriction changes with the dynamic field, resulting in the ultrasonic source. The magnetostriction constant $e_{k,ij}$ represents the dynamic response of the magnetostriction stress σ_{ij} to the field H_k. Using the magnetostriction ε_{mn} which depends on the total field, $e_{k,ij}$ is expressed as

$$e_{k,ij} \equiv \frac{\partial \sigma_{ij}}{\partial H_k} = \frac{\partial \sigma_{ij}}{\partial \varepsilon_{mn}}\bigg|_{H=0} \frac{\partial \varepsilon_{mn}}{\partial H_k}\bigg|_{\sigma=0} \tag{24}$$

where $\left.\frac{\partial \sigma_{ij}}{\partial \varepsilon_{mn}}\right|_{H=0}$ can be replaced by the elastic stiffness.

When the dynamic field is superimposed on the static bias field, the total field is inclined from the original direction. Because the dynamic electromagnetic amplitude is much smaller than the static ones, and the static bias field is in z direction, only three principal stresses (σ_{11}, σ_{22}, and σ_{33}) exist. On the iso-volume magnetostriction and small ultrasonic amplitude assumptions, the magnitude of the magnetostriction along the applied field (z) is two times larger than those in the perpendicular direction (x, y), being in the opposite sign. Eq. (24) is reduced to

$$\left.\begin{aligned} \frac{\partial \sigma_{11}}{\partial H_1} &= 6kG \\ \frac{\partial \sigma_{22}}{\partial H_1} &= -3kG \\ \frac{\partial \sigma_{33}}{\partial H_1} &= -3kG \end{aligned}\right\} \tag{25}$$

where G is the shear modulus and $k = \frac{\partial \varepsilon_{11}}{\partial H_1}$ is a function of the total field and given from the slope of the magnetostriction curve in Fig. 3. The magnetostriction constant can be obtained for the normal field as

$$\left.\begin{aligned} e_{1,11} &= 6kG, \quad e_{1,13} = 0 \\ e_{1,33} &= -3kG, \quad e_{3,11} = -3kG \\ e_{3,13} &= 0, \quad e_{3,33} = 6kG \end{aligned}\right\} \tag{26}$$

The magnetostriction force is determined by

$$\boldsymbol{f}_{MS}^{i} = \frac{\partial \sigma_{ij}}{\partial x_j} = e_{k,ij}\frac{\partial H_k}{\partial x_j} \tag{27}$$

According to Eqs. (1) and (5), once the body force is obtained, the ultrasonic amplitude $\boldsymbol{u}$ can be obtained through a numerical way according to Eq. (5).

4 Numerical Calculations

All numerical calculations are conducted according to the aforementioned equations. The conductor width d is ignored compared with wire space b ($d \ll b$). When applying the numerical method for eddy current and Lorentz force calculation, the total number of turns is $2k = 10$, and other parameters are as follows: $f = 2$ MHz, $b = 2$ mm, $l = 20$ mm, $h = 0.5$ mm, $I_0 = 30$ A, $G = 80$ GPa, $\sigma = 3.3$ MS/m, $\mu_0 = 1.26$ μH/m, $\mu_1 = 1$, $\mu_2 = 2\,200$, and $H_0 = 1$ Oe.

Figs. 4 − 6 show the components of eddy current density in x, y and z directions in the metal surface at

$t = 1$ μs, respectively. Note the eddy currents in x and z directions occur only at the two edges (front and back) of the coil and are much smaller than those in y direction about 50 dB which will dominate the EMAT phenomena when only concerned with the Lorentz force mechanism. This results in the Lorentz force being much larger in x direction than those in y and z directions. The resulting eddy current distribution shown in Fig.5 reveals the increased magnitude of the eddy current density at the two free ends (left and right) of the meandering coil.

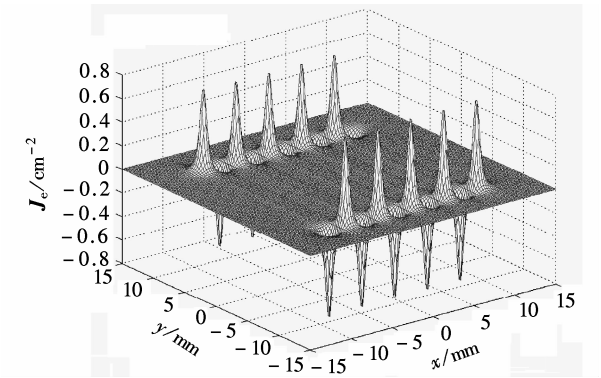

Fig.4 x-component of induced eddy current on the metal surface

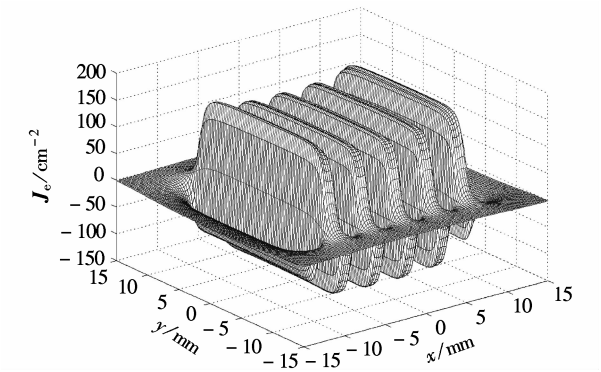

Fig.5 y-component of induced eddy current on the metal surface

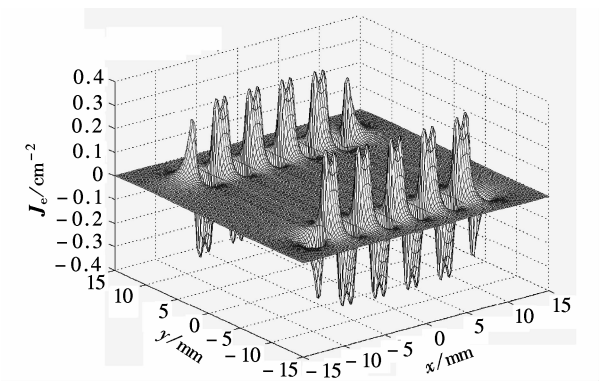

Fig.6 z-component of induced eddy current on the metal surface

Fig. 7 shows the y-component of induced eddy current on the section of $y = 0$ plane at $t = 1$ μs, $f = 2$ MHz, with a lift-off 0.5 mm. It is indicated that deep into the inspected material the eddy current density will decrease dramatically because of the skin effect.

According to Eqs. (20) and (21), the x-component of Lorentz force and magnetization force can be calculated and then the corresponding stresses are shown in Figs.8 and 9. Pay attention to that the stress generated by the Lorentz force is much stronger than the one due to magnetization force in this direction and will make a main contribution for ultrasonic generation. With the same numerical method, the Lorentz force and the magnetization force in other directions are obtained.

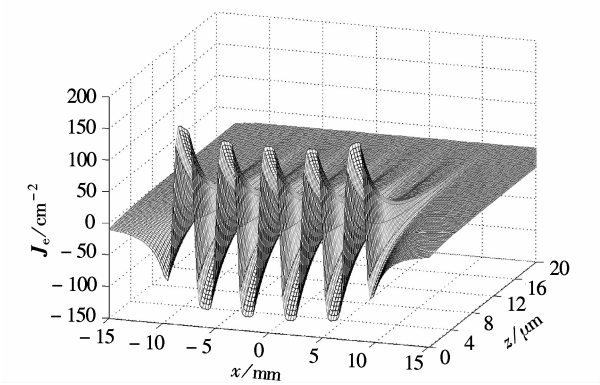

Fig. 7 y-component of induced eddy current on the section of $y = 0$ plane

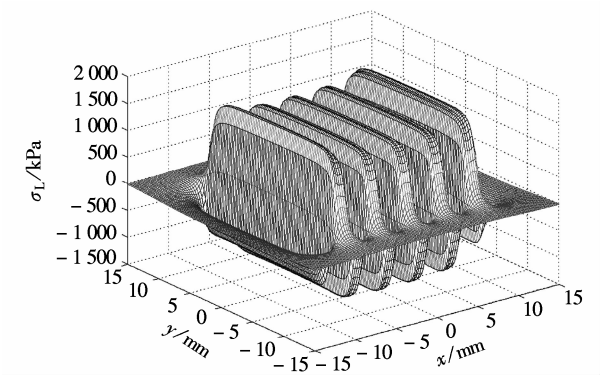

Fig.8 x-component stress generated by Lorentz force on the metal surface

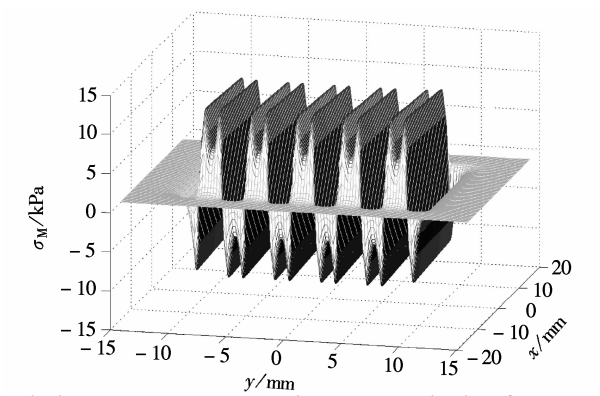

Fig.9 x-component stress due to magnetization force on the metal surface

Once the magnetostriction force is obtained under the condition that the magnetization curve of the metal

is known, the corresponding stresses can be calculated. Fig.10 shows the relation between magnetostriction stress and bias magnetic field. It is indicated that with the bias magnetic field increasing the magnetostriction stress decreases nonlinearly and vanishes when the magnetizing reaches saturation. Another calculation of the magnetostriction stress on $y = 0$ plane at $t = 1$ μs, $f = 2$ MHz, with a lift-off 0.5 mm and bias magnetic field 200 Oe is shown in Fig. 11. Note the difference between Fig.11 and Fig.7.

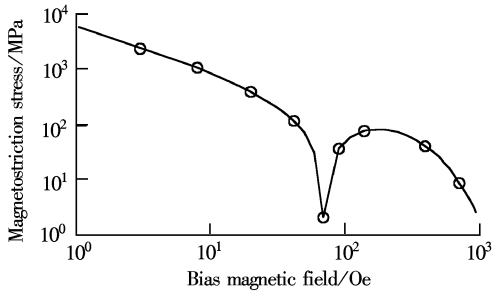

Fig.10 The relation between magnetostriction stress and bias magnetic field

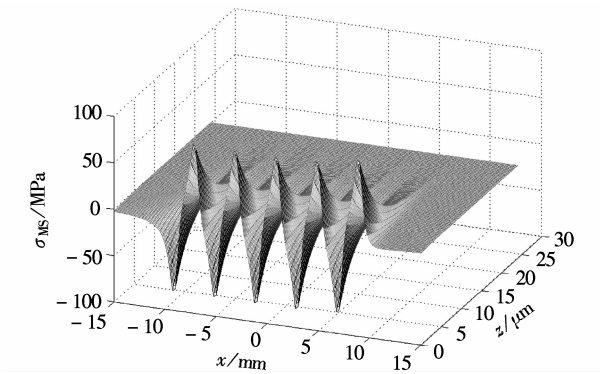

Fig.11 Amplitude of magnetostriction stress on $y = 0$ plane with a bias magnetic field 200 Oe

Fig.12, where u_0 means the unit of ultrasonic amplitude at $B_0 = 1$ Oe due to the Lorentz force mechanism, indicates a much larger contribution of the magnetostriction effect than others, especially in the lower field region. As the external field increases, the contributions of the Lorentz force and the magnetization force become considerable. But, after the metal reaches saturation, the Lorentz force effect will **not increase while the external field increases.**

5 Conclusions

The numerical method has been used to evaluate the eddy current distribution, body force and ultrasonic amplitude for EMAT. Based on the discussion of the mechanisms for EMAT phenomena, several useful conclusions can be derived from the calculation.

1) The Lorentz force mechanism can be seen as the only mechanism for nonferromagnetic material

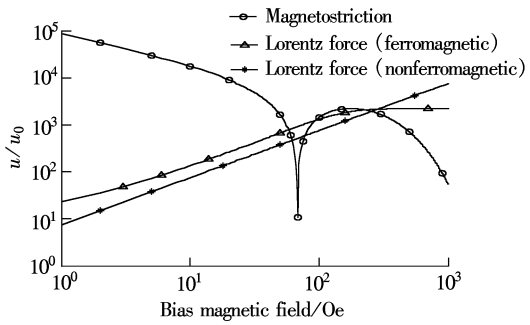

Fig.12 Dependence of the ultrasonic amplitude generated electromagnetically in a metal with the bias magnetic field

because the other two forces are very small and their influences can be neglected, resulting in a good linearity.

2) When inspecting ferromagnetic conducting material, the electromagnetic field can change the magnetostrictive coefficient of the material. The magnetostriction force lies on not only the amplitudes and directions of the bias static magnetic field, but also the magnetic domain distribution of the material. The magnetostriction effect can intensify the ultrasonic while the intensity of the static magnetic field is low. But, with the bias magnetic field increasing and saturation, the magnetostrictive terms will make no contributions to the ultrasonic generation. The Lorentz force becomes the only exciting mechanism, and will saturate when the material reaches its magnetizing saturation. In this case, the only way for getting higher ultrasonic amplitude is to increase the source current density in the EMAT coil. It is important to determine both the Lorentz and magnetostriction forces and select the appropriate working manner for achieving an optimized design.

3) As the skin depth for ferromagnetic material is usually smaller than nonferromagnetic ones according to Eq.(16), for example, the skin depth is 38 μm for aluminum and 1.8 μm for steel at a frequency 5 MHz, the surface conditions, such as roughness, coating, oxidizing, and so on, will affect the eddy current distribution more easily. If the surface conditions are not good, it is much harder to excite ultrasonic using the Lorentz force mechanism. So, most EMATs for ferromagnetic material inspection are based on magnetostriction effect.

Future work is to model EMAT receivers so that the entire nondestructive inspection system can be optimized for better detection and characterization of a **specified flaw type.**

References

[1] Schramm Raymond E. Ultrasonic measurement of stress in

railroad wheels [J]. *Review of Scientific Instruments*, **1999, 70**(2): 1468 - 1472.
[2] Tittmann B, Alers R, Lerch R. Ultrasonics for locomotive wheel integrity [A]. In: Schneider S C, Levy M, eds. *IEEE Ultrasonics Symposium Proceedings* [C]. Milwaukee, WI: Alejandro Zajacl Sawtek, Inc, 2000. 743 - 746.
[3] Hirao Masahiko, Ogi Hirotsugu. An SH-wave EMAT technique for gas pipeline inspection [J]. *NDT & E International*, **1999, 32**(3): 127 - 132.
[4] Boulavinov Andrei, Kroening Michael, Nikiforenko George. Phase controlled EMAT antenna for the inspection of coated pipes [EB/OL].http: //www.nde2002.org/papers/089P.pdf. 2002-12-05/2003-12-07.
[5] Miller Matthew, Mi Bao, Kita Akio, et al. Development of automated real-time data acquisition system for robotic weld quality monitoring [J]. *Mechatronics*, **2002, 12**(9, 10): 1259 - 1269.
[6] Murayama Riichi, Fujisawa Kazuo, Fukuoka Hidekazu, et al. Development of an on-line evaluation system of formability in cold-rolled steel sheets using electromagnetic acoustic transducers (EMATs) [J]. *NDT & E International*, **1996, 29**(3): 141 - 146.
[7] Ogi Hirotsugu, Hamaguchi Takayuki, Hirao Masahiko. In-situ monitoring of ultrasonic attenuation during rotating bending fatigue of carbon steel with electromagnetic acoustic resonance [J]. *Journal of Alloys and Compounds*, **2000, 310**(1, 2): 436 - 439.
[8] Ogi Hirotsugu. Field dependence of the coupling efficiency between electromagnetic field and ultrasonic bulk waves [J]. *J Appl Phys*, **1997, 82**(8): 3940 - 3949.
[9] Ludwig R, Dai X W. Numerical simulation of electromagnetic acoustic transducer in the time domain [J]. *J Appl Phys*, **1991, 69**(1): 89 - 97.
[10] Murayama Riichi. Study of driving mechanism on electromagnetic acoustic transducer for Lamb wave using magnetostrictive effect and application in drawability evaluation of thin sheets [J]. *Ultrasonics*, **1999, 37**(1): 31 - 38.

铁磁材料中基于电磁声换能器的超声发射机理研究

雷华明　阙沛文　张志钢　黄　晶

(上海交通大学自动检测研究所, 上海 200030)

摘要: 基于适当的假设和近似, 通过分析电涡流的分布、洛伦兹力、磁致伸缩力和磁化力, 研究了在铁磁材料中用电磁声换能器(EMAT)的方法产生超声的耦合机理, 并针对有实用意义的结构参数进行了数值计算以解释换能器的性能. 结果表明: 对于铁磁性材料, 在磁场强度较低、材料磁化未达到饱和时, 磁致伸缩效应在 EMAT 超声波的产生中起主导作用; 但是, 随着偏置磁场的逐渐增强而使材料达到磁化饱和时, 磁致伸缩逐渐消失, 对产生超声不再有贡献作用, 洛伦兹力变成是激发超声的惟一原因. 因此, 为获得优化的设计, 计算洛伦兹力和磁致伸缩力以及选择合适的工作方式变得尤为重要.

关键词: 电磁声换能器; 铁磁材料; 超声发射; 电涡流; 洛伦兹力; 磁致伸缩力

中图分类号: TB5